Backbone dynamics of complement control protein (CCP) modules reveals mobility in binding surfaces

Backbone dynamics of complement control protein (CCP) modules reveals mobility in binding surfaces

JOANNE M. O'LEARY,[1,2] KRYSTYNA BROMEK,[1] GORDON M. BLACK, STANISLAVA UHRINOVA, CHRISTIAN SCHMITZ,[3] XUEFENG WANG,[4] MALGORZATA KRYCH,[4] JOHN P. ATKINSON,[4] DUSAN UHRIN, AND PAUL N. BARLOW

Schools of Chemistry and Biology, University of Edinburgh, Edinburgh EH9 3JJ, Scotland

(RECEIVED December 18, 2003; FINAL REVISION January 27, 2004; ACCEPTED February 1, 2004)

Abstract

The regulators of complement activation (RCA) are critical to health and disease because their role is to ensure that a complement-mediated immune response to infection is proportionate and targeted. Each protein contains an uninterrupted array of from four to 30 examples of the very widely occurring complement control protein (CCP, or sushi) module. The CCP modules mediate specific protein–protein and protein–carbohydrate interactions that are key to the biological function of the RCA and, paradoxically, provide binding sites for numerous pathogens. Although structural and mutagenesis studies of CCP modules have addressed some aspects of molecular recognition, there have been no studies of the role of molecular dynamics in the interaction of CCP modules with their binding partners. NMR has now been used in the first full characterization of the backbone dynamics of CCP modules. The dynamics of two individual modules—the 16th of the 30 modules of complement receptor type 1 (CD35), and the N-terminal module of membrane cofactor protein (CD46)—as well as their solution structures, are compared. Although both examples share broadly similar three-dimensional structures, many structurally equivalent residues exhibit different amplitudes and timescales of local backbone motion. In each case, however, regions of the module-surface implicated by mutagenesis as sites of interactions with other proteins include several mobile residues. This observation suggests further experiments to explore binding mechanisms and identify new binding sites.

Keywords: CCP module; SCR; complement; backbone dynamics; NMR

Proteins composed of trains of modules are widespread, especially in the extracellular environment, and they are functionally diverse (Bork et al. 1996). The regulators of complement activation (RCAs) are biologically important examples of multiple-module proteins (for review, see Kirkitadze and Barlow 2001). Members of this family act in an orchestrated fashion to ensure that a complement-mediated immune response is proportionate, directed against the pathogen, and coordinated with other arms of the immune system (for review, see Walport 2001). RCAs exercise discrimination between self and nonself through their association with host-specific cell-surface glycosaminoglycans (Pangburn 2000), or by virtue of being inserted within

Reprint requests to: Paul Barlow, Schools of Chemistry and Biology, Joseph Black Chemistry Building, University of Edinburgh, West Mains Road, Edinburgh, EH9 3JJ, Scotland; e-mail: Paul.Barlow@ed.ac.uk; fax: 44-1-31-650-7055.

[1]These authors contributed equally to this work.

Present addresses: [2]Department of Biochemistry, University of Oxford, OX1 3Q4, UK; [3]Biophysical Chemistry Group, Institute of Physical Chemistry, University of Heidelberg, D-69120, Germany; [4]Washington University School of Medicine, St. Louis, MO 63110, USA.

Abbreviations: CCP, complement control protein; CR1, complement receptor type 1; MCP, membrane cofactor protein; NOE(sy), nuclear Overhauser effect (spectroscopy); NMR, nuclear magnetic resonance spectroscopy; RCA, regulators of complement activation; rms, root mean square; TOCSY, total correlation spectroscopy.

Article and publication are at http://www.proteinscience.org/cgi/doi/10.1110/ps.03582704.

(Liszewski et al. 1991) or anchored to (Medof et al. 1987) the host plasma membrane. RCA proteins inactivate C3- and C5-convertases that assemble on self cell-surfaces. Inactivation may be reversible if the convertases are dissociated into their intact subunits, or irreversible if C3b and C4b subunits are proteolyzed by factor I with an RCA protein acting as a cofactor. In either case, binding of an RCA protein to C3b and/or C4b subunits is critical. Both membrane cofactor protein (MCP) and complement receptor type 1 (CR1) are efficient cofactors for factor I, whereas CR1 also accelerates convertase-dissociation. Erythrocyte-borne CR1 additionally performs an essential role in clearance from the human bloodstream of C3b- or C4b-coated pathogens and immune complexes (Birmingham and Herbert 2001).

This functional sophistication, entailing both structural and specific binding roles, derives from apparent compositional simplicity because the most common variants of RCA proteins are each composed entirely, or almost entirely, from between four and 30 examples of a single module type, the complement control protein (CCP) module (Reid and Day 1998)—also known as a short consensus repeat or sushi domain. CCP modules contain ~60 residues each and are most abundant within proteins of the complement system but are found also in a large number of other, functionally diverse proteins (http://smart.embl-heidelberg.de/). The CCP module has an elongated structure with C and N termini positioned at opposite ends. Loops, bulges, and turns account for ~50% of the amino acid sequence, and the remainder forms short β-strands. In most examples that have been studied, sequential modules are arranged end-to-end with only a small intermodular contact surface (Barlow et al. 1993; Kirkitadze et al. 1999b; Henderson et al. 2001; Murthy et al. 2001; Smith et al. 2002; Uhrinova et al. 2003; Williams et al. 2003).

Mobility both between and within individual modules contributes to conformational flexibility and physical properties, which may be critical for function of a multiple-module protein. More generally, there are many examples of proteins in which local mobility occurs in those regions of the protein surface that are involved in specific intermolecular contacts (for review, see Ishima and Torchia 2000; Wand 2001). Although past efforts have been directed toward elucidating mobility *between* CCP modules (Kirkitadze et al. 1999a,b,c; Henderson et al. 2001), there is little information available on backbone motion within the modules. Although some ^{15}N-relaxation data were reported for CCP modules previously (Smith et al. 2002; Uhrinova et al. 2003), they were not analyzed in detail. NMR has now been used for the first time to characterize backbone motions in these very widely occurring modules. Here we report solution structures and analyze, by using the model-free approach, the ^{15}N relaxation parameters of two diverse (20% identity) examples—the 16th module of CR1 (CR1~16), and the N-terminal module of MCP (MCP~1). The CR1 example lies within the 30 CCP-extracellular portion of this transmembrane glycoprotein and is the central module of the biologically critical functional site 2, namely, modules 15–17, that binds C3b and C4b (a second copy of site 2 is present in modules 8–10 of CR1; for review, see Krych-Goldberg and Atkinson 2001). MCP~1, in contrast, is at the membrane-distal N terminus of the extracellular portion of this smaller transmembrane glycoprotein. MCP~1 forms part of the C4b-binding region of MCP (Liszewski et al. 2000) and is half of the site that is recognized by the measles virus (Manchester et al. 1997; Hsu et al. 1999).

The current work shows that despite their broadly similar three-dimensional (3D) structures, there are significant differences in backbone motion between these two examples of CCP modules. A shared feature, however, appears to be the presence of mobile residues at the respective binding surfaces of the two modules.

Results

The solution structures of the individual modules

3D structures of both these modules in the contexts of longer fragments of their respective parent proteins have been solved previously (Casasnovas et al. 1999; Smith et al. 2002). It could not be assumed, however, that the 3D structures of the modules would be the same when expressed as individual units. To ensure that analysis of relaxation data was based on appropriate 3D structures, full backbone and side-chain assignments of ^{15}N-labeled samples of CR1~16 and MCP~1 were undertaken as a basis for nuclear Overhauser effect (NOE)-based structure determinations (Table 1; Fig. 1).

Figure 2 shows the ensembles of 20 calculated solution structures for MCP~1 and CR1~16, selected on the basis of lowest NOE violation energy. Also shown is an overlay of the closest-to-the-mean structure of each module with the previously determined structures of the module-pairs CR1~15,16, CR1~16,17 (Smith et al. 2002), and MCP~1,2 (Casasnovas et al. 1999). Allowing for the lack of precision that is a consequence of dynamic events (see below) and the limitations of the data, there are only very minor structural differences between the published module structures and the individual ones calculated here; these differences are restricted to loops and turns that lie proximal to intermodular junctions.

Comparison of structures of MCP~1 and CR1~16

Similar to all CCP modules studied to date, MCP~1 and CR1~16 share a common structural framework (Figs. 1A, 2B). β-Strand B, however, starts later in CR1~16 than in MCP~1, and its partner strand D is extended by two resi-

Table 1. *NMR structure determination statistics*

	MCP-1	CR1–16
Total NOEs used for CNS calculation	1441	885
Intraresidue NOEs	426	348
Sequential	362	192
Short range, 2 = <li-j< = 4	132	36
Long range, li-jl>4	521	181
Hydogen bonds	16	—
Structure calculation stats. (20 structures out of 60)		
No. of NOE violations >0.5 Å[a]	0	0
Procheck statistics		
Residues in most favored region (%)	57.6	64.0
Residues in additional allowed regions (%)	32.2	31.3
Residues in generously allowed regions (%)	8.5	3.5
Residues in disallowed regions (%)	1.7	1.2
rmsd from the experimental restraints[b]		
NOEs (Å)	0.039 ± 0.005	0.016 ± 0.001
J restraints (°)	0.79 ± 0.05	—
rmsd from idealised geometry[a,b]		
Bond lengths (Å)	0.0034 ± 0.0001	0.0010 ± 0.0002
Bond angles (°)	0.44 ± 0.016	0.24 ± 0.01
rmsd from the average structure (Å)[c]		
Backbone atoms (all native)	0.97	1.03
Backbone atoms (CysI-CysIV)	0.56	0.94

[a] The number given is the accumulated total for all 20 structures in the ensemble.
[b] Number is mean ± SD.
[c] Numbers are average deviations for atoms N, C^{α}, C, O.

dues; consequently, the DE loop is shorter in MCP~1 and has a different orientation to its equivalent in CR1~16 (Fig. 1B). Other differences arise from insertions and deletions—for example, two residues inserted within the hypervariable loop of MCP~1 (between strands B and D) are evident in the 3D structure, as are the bulges in MCP~1 caused by insertion of two amino acids between β-strands E and F; the three amino acid residues inserted between strands F and G of CR1~16 produce a more prominent FG loop. The four-stranded sheets that form the central portions of the two modules overlay well—1.57 Å over 27 residues (as shown in Fig. 2; residues used for overlay indicated in Fig. 1A). The bottom and, particularly the top of the modules—as drawn in Figure 1B—are, however, significantly different; the root mean square deviation is 2.42 Å if the EH sheet is included in the comparison.

Relaxation measurements

In ^{15}N NMR relaxation studies, the motional probes, that is, the NH pair of nuclei, are present in virtually all residues. In addition to prolines, the only residues totally excluded from analysis are those with resonances that are overlapped within the spectra. If a specific signal is too weak to be integrated reliably and analyzed, this is normally due to particular dynamical features of the residue concerned, and some degree of information may still be inferred. Three MCP~1 residues (Ile22, Arg25, and Lys32) gave overlapped HSQC signals, whereas the Cys30 and Thr51 peaks were too weak to measure accurately, and no resonance due to Asn49 (the site of an N-acetylglucosamine attachment) was present in the spectrum. The analysis of Trp52 in MCP~1 is taken from its side chain NH bond parameters due to overlap (and weakness) of its backbone signal. In CR1~16, Met973 and Cys990 produced overlapped HSQC signals, whereas peaks were absent for a further three residues (Gly993, Gly1008, and Asn1009). Relaxation data and heteronuclear NOEs for both CCPs are shown in Figure 3—the N termini consisting of expression artefacts, and with highly elevated ^{15}N relaxation times, are not included. Figure 3 also includes data for module 16 within the contexts of the module pairs, that is, $^{(15)}16$ and $16^{(17)}$, and crystallographic B-factors (averaged over six structures in the unit cell) for MCP~1 (Casasnovas et al. 1999).

Heteronuclear NOEs

Although ^{15}N relaxation data have been previously reported for CCP module-pairs (Smith et al. 2002; Uhrinova et al. 2003), model-free analysis (Lipari and Szabo 1982) of the data, which allows motion on several timescales to be probed, had failed due to the possible influence of inter-modular motion on the apparent anisotropy of diffusion. Incorrect assumptions of anisotropy for a system that is

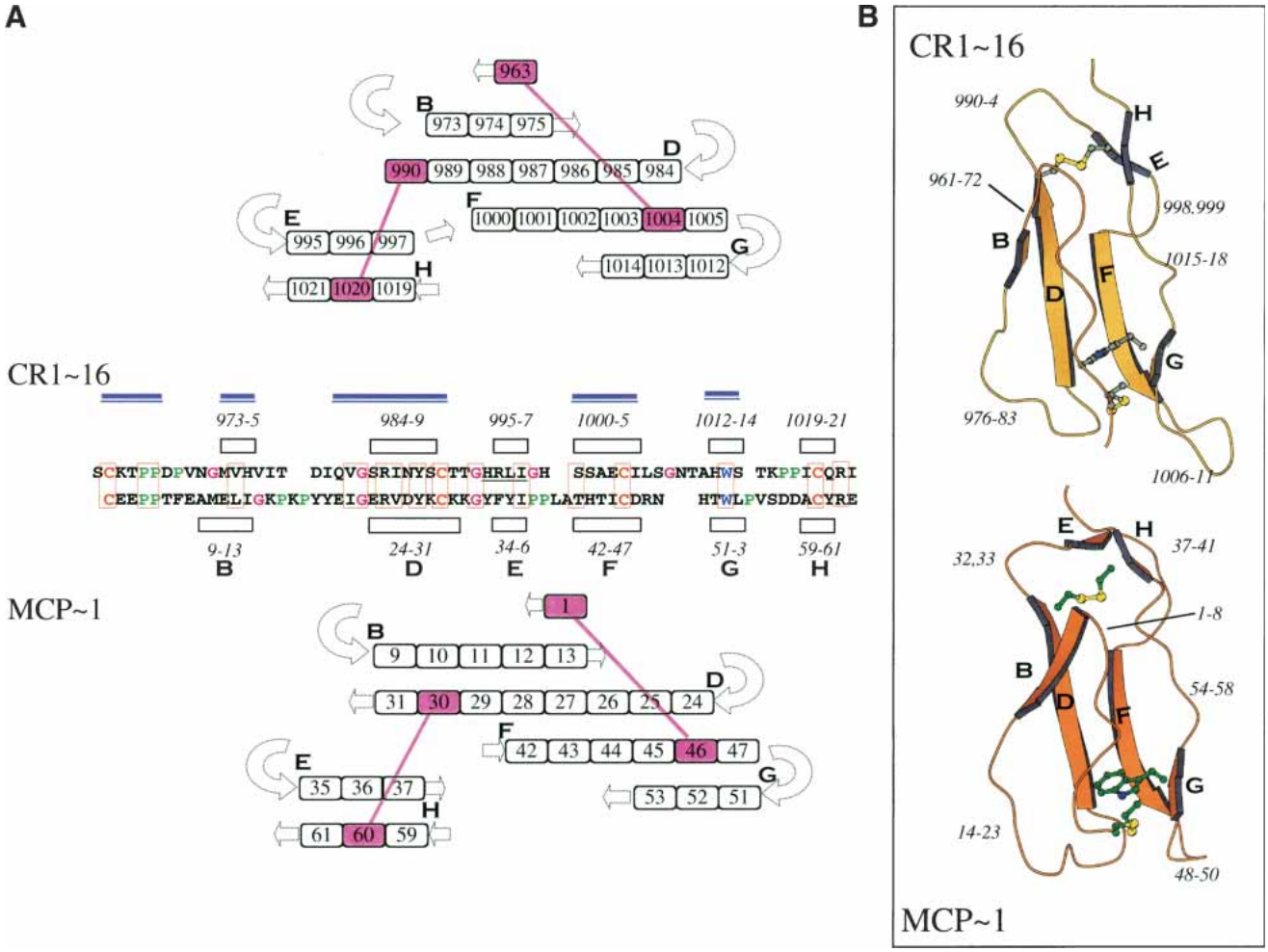

Figure 1. Sequence alignment and structural comparisons. (*A*) (*Center*) Sequence-alignment of CR1~16 and MCP~1, numbered according to native sequences of parent proteins. Identities/conservative replacements indicated by boxes (Asn987 is mutated to Thr in the CR1~16 used for this study). Position and annotation (B, D, E–H) of β-strands in each module is shown by white rectangles immediately *above/below* sequence alignment. Regions used for superposition of 3D structures are indicated by the double line above the CR1~16 secondary structure. (*Top*, *bottom*) Arrangement of annotated strands (residues indicated by sequence numbers). Cysteines are shaded and di-sulphides indicated. (*B*). MOLSCRIPT (Kraulis 1991) representations of NMR-derived structures of CR1~16 and MCP~1. Views shown are equivalent (based on superposition using regions indicated in *A*). Strands annotated as in *A*; nonstrand regions are labeled with residue numbers; side chains of consensus Cys and Trp are drawn as ball-and-stick.

potentially highly elongated could lead to inappropriate choice of motional models. Hence, the full analysis of backbone dynamics for single CCP modules presented below provides the first detailed picture of motion in this module type. Inspection of the raw ^{15}N relaxation data for the single modules also contributes to the current study because it allows a direct comparison between data collected on the individual module 16 and data collected on the same module but in the context of longer fragments (Fig. 3; Smith et al. 2002). This is important because it addresses the question of whether observations made on single modules are relevant to the multiple-module parent protein.

The magnitude of the heteronuclear NOE (Fig. 3A,B) is sensitive to backbone mobility on the 10^{-8} to 10^{-12} sec timescale, with higher sensitivity for the slower and larger amplitude motions. It also depends on the overall rotational correlation time, and for structured residues, the expected value of the ^{1}H-^{15}N NOE can be calculated for CR1~16 and MCP~1 to be ~0.67, whereas for CR1~15,16 or CR1~16,17 the expected value is ~0.70 (Kay et al. 1989; Mandel et al. 1995). The difference between the average measured heteronuclear NOE of CR1~16 (0.67 ± 0.05) and of the same module within the contexts of the pairs CR1~$^{(15)}$16 or CR1~16$^{(17)}$ (0.71 ± 0.05 and 0.71 ± 0.07, respectively) is therefore within the range expected due to the larger size of the double module and does not imply that overall the internal 10^{-8} to 10^{-12} sec mobility of the single module is significantly different from that of the same module within

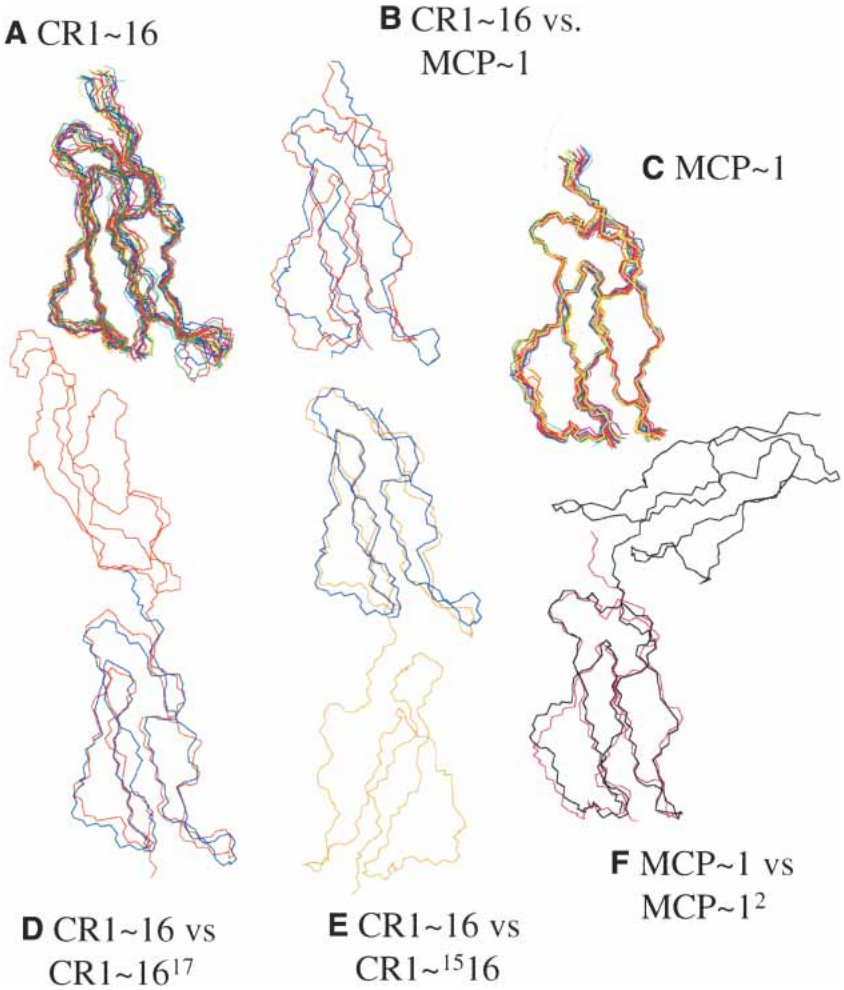

Figure 2. Comparison of module structures in various contexts. All structures are shown as overlays of backbone traces. (*A*) Ensemble of 20 NMR-derived CR1~16 structures. (*B*) Closest-to-the-mean NMR-derived structures of CR1~16 (blue) vs. MCP~1 (red). (*C*) Ensemble of 20 NMR-derived MCP~1 structures. (*D*) Closest-to-the-mean structures of CR1~16 vs. CR1~16$^{(17)}$. (*E*) Closest-to-the-mean structures of CR1~16 and CR1~$^{(15)}$16. (*F*) Closest-to-the-mean MCP~1 structure with the X-ray–derived MCP~1,2 structure.

a pair. Residues within loops and located at the ends of strands proximal to the N terminus of CR1~16 have heteronuclear NOE values lower than the module-average, and a similar trend is discernible in CR1~16$^{(17)}$. Likewise, those residues found in loop GH and strand H of CR1~16 (Fig. 1), which are near the C terminus and would be in the vicinity of the interface with module 17, have lowered heteronuclear NOEs, similar to the equivalent residues in CR1~$^{(15)}$16. Otherwise, there are few obvious differences between the heteronuclear NOEs of CR1~16, CR1~$^{(15)}$16, and CR1~16$^{(17)}$. The ^{15}N longitudinal and transverse relaxation times (T_1 and T_2; Fig. 3D,F) for module 16 also exhibit similar trends in all three contexts. Thus, the backbone dynamics of the individual module, similar to its 3D structure, appear to be independent of the presence of neighboring modules with the exception of loops near intermodular junctions. No such comparison of dynamics is available for MCP~1 (Fig. 3C,E), although inspection of crystallographic B-factors might be expected to yield some insight into local motion within the crystal lattice. As Figure 3A illustrates, however, equivalent residues of the six MCP~1,2 molecules within a unit cell exhibit a range of B-factors, presumably due to various crystal contacts, and it is not possible to attach any significance to the lack of correlation between thermal motion in crystalized MCP~1,2 and heteronuclear NOEs, ^{15}N T_1s or ^{15}N T_2s of MCP~1 in solution.

Model-free analysis

As a basis for extended model-free analysis of relaxation data, the NMR-derived structures of MCP~1 and CR1~16 were used initially to establish overall rotational diffusion. In both cases, diffusion was best represented by isotropic correlation times (Table 2), despite the elongated nature of

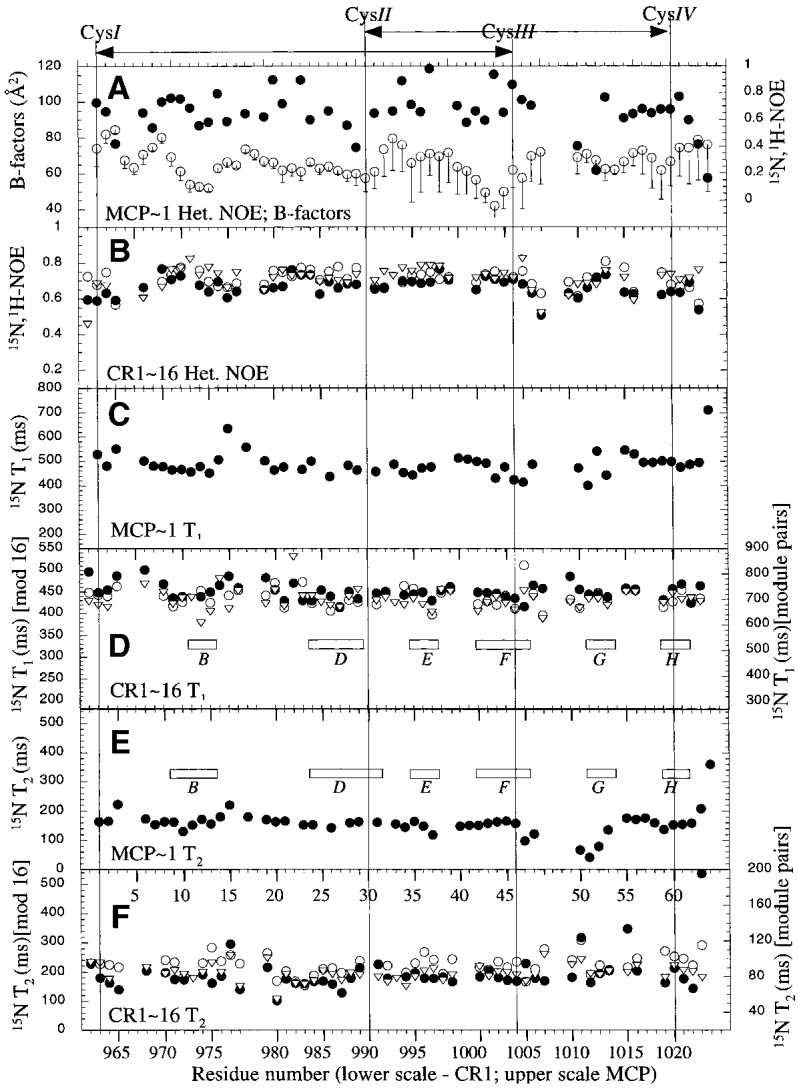

Figure 3. Comparison of relaxation data. Relaxation data plotted vs. residue numbers (see *X*-axes of lower two panels) for both modules so as to line up equivalent residues according to alignment in Fig. 1A. Positions of Cys residues and di-sulphides are shown. Except for B-factors, error bars lie within the boundaries of the symbols. (*A*) MCP~1 het NOEs (●, *right* axis) compared with mean B-factors (○, *left* axis)—half-error bars on B-factors correspond to standard deviation over six structures. (*B*) CR1~16 het NOEs (●, CR1~16; ▽, CR1~16[17]; ○, CR1~[15]16). (*C*) MCP~1 T_1 values. (*D*). CR1~16 T_1 values (●, CR1~16, *left* axis; ▽, CR1~16[17], *right* axis; ○, CR1~[15]16, *right* axis). Rectangles are schematic representation of the CR1~16 β-strands. (*E*) MCP~1 T_2 values. Rectangles are schematic representations of the MCP~1 β-strands. (*F*) CR1~16 T_2 values (●, CR1~16, *left* axis; ▽, CR1~16[17], *right* axis; ○, CR1~[15]16, *right* axis).

the modules that is apparent by inspection. Subsequently, the alternative structure of MCP~1 derived from the crystal structure of MCP~1,2 was used instead of the solution structure. Although the crystal structure does not, overall, significantly differ from the NMR-derived structure, it shows greater variation in the distribution of NH bond vector directions and a better correlation to the T_1/T_2 ratios. This resulted in a significant improvement of the fit with axially symmetric diffusion, yielding a $D_{||}/D_{\perp} = 1.35$, a value that is close to the modelled axial ratio, which = 1.6.

Subsequently, relaxation data for MCP~1 (or CR1~16) were analyzed based on symmetric (or isotropic) diffusion to assign a specific model (Lipari and Szabo 1982) to each residue by adopting the extended model-free approach (Fig. 4). The five allowed models, 1–5, are parameterized as follows: (1) S^2; (2) S^2, τ_e; (3) S^2, R_{ex}; (4) S^2, τ_e, R_{ex}; and (5) S^2, S_f^2, τ_e. The square of the order parameter, S, correlates with the spatial restriction of the NH bond vector, and ranges between zero for isotropic internal motions and unity for completely restricted internal motion. Model 1 ad-

Table 2. *Diffusion parameters calculated for MCP-1 and CR1-16*

	MCP-1 Diffusion model			CR1-16 Diffusion model
	Isotropic[a]	Ax. symm (NMR)[b]	Ax. symm (X-ray)	Isotropic[a]
τ_c [ns]	4.51 ± 0.01	4.49 ± 0.01	**4.50 ± 0.01**	3.65 ± 0.01
$D_\parallel D_\perp$	1	1.19 ± 0.02	**1.35 ± 0.02**	—
θ[°][c]	—	15 ± 2	**14 ± 2**	—
ϕ[°][c]	—	159 ± 1	**−111 ± 2**	—
$\chi^2_{reduced}$	—	3.96	**3.08**	—
F_{exp} (5%)[d]		−	+	

The parameters of the accepted models of diffusion are presented in bold.

[a] $\tau_c = (6\mathrm{Tr}(D))^{-1}$, does not require structural input.

[b] The nearest-to-mean structure from the NMR ensemble was used in the fitting.

[c] In the axially symmetric model, θ is defined as an angle between I_z and $D_\parallel$, and ϕ as an angle between I_x and the projection of $D_\parallel$ onto the XY plane.

[d] + and − indicate that the experiment value of F_{exp} classifies the improvement as significant at a 95% level of probability.

equately describes the experimental data only when internal motions are very fast—otherwise an internal correlation time, τ_e (model 2), is added. Models 3 and 4 are equivalent to models 1 and 2, respectively, with addition of a chemical exchange contribution, R_{ex}, reflecting T_2 relaxation due to the slowest analyzed (10^{-9} to 10^{-6} sec timescale) motion. In model 5 $S^2 = S_f^2 S_s^2$, where S_f is the generalized order parameter for internal motion on the very fast timescale of a few picoseconds that does not require fitting of an accompanying τ_e, and S_s is the order parameter for slow (~1 nsec) timescale motion accompanied by a fitted τ_e.

In the case of CR1~16, no suitable dynamical model was found for seven residues (Fig. 4) within the overall isotropic model of diffusion despite them having resolved HSQC peaks. All except two of the MCP~1 residues judged suitable for analysis were fitted by using one of the five dynamical models, with the more complicated models 4 and 5 used for nine residues. Figure 4 shows a comparison of the model-free derived data for the two modules plotted as a function of residue number.

The average value of S^2 in MCP~1 is 0.79 ± 0.10 (excluding two C-terminal residues). The order parameters are less variable than are measured heteronuclear NOEs (Fig. 3A) probably because the S^2 calculations also take into account the relaxation times, which can be measured with higher precision, and are a relatively accurate monitor of 10^{-12} to 10^{-9} sec timescale mobility. Strands with the exception of strand G generally have order parameters higher than average (Fig. 4). Tyr29 in strand D is a clear outlier with a moderately lowered S^2, 0.71 ± 0.02, corresponding to its low heteronuclear NOE, but a relatively long internal correlation time τ_e, 604 ± 109 psec.

S^2 values for CR1~16 have a higher average value of 0.82 ± 0.04. The β-strands of CR1~16 have remarkably consistent average S^2 values (Fig. 4) with, in general, very little variation within strands. Thus, from order parameters, the picture emerges of CR1~16 as having a framework-like structure composed of mainly rigid (on the 10^{-12} to 10^{-9} sec timescale) β-strands, whereas MCP~1 is more dynamic.

A comparison (Fig. 4) of order parameters of equivalent amino acid residues (based on the alignment in Fig. 1A) in the two individual modules reveals significant discrepancies for some pairs of residues. The most obvious examples (differences <0.1 underlined) in which the MCP~1 residue has a lower value are Cys1/Cys963, Glu3/Thr965, Leu12/Val974, and Glu24/Ser984. Examples of comparisons in which the CR1~16 residue has a lower value are Ile986/Val26, Tyr988/Tyr28, Ile997/Ile37, Leu1006/Arg48, and Ser1014/Leu53. There are other pairs of equivalent (in the alignment) residues in which the data could be fitted for one module (normally MCP~1) but not the other. The differences in motion between the two modules are not limited to loops and turns or other regions that are not structurally conserved. For example, two of these discrepancies (Glu24/Ser984 and Ile986/Val26) are in the portion of strand D that is common to both modules and is well conserved in terms of structure and sequence (Fig. 1A).

Among 24 MCP~1 amino acids that exhibit motion on a timescale slower than a few picoseconds, and which therefore require τ_e, there are five residues undergoing a two-mode 10^{-12} to 10^{-9} sec timescale motion. The fast component is then described by S^2_f, and the slow component by S^2_s, along with τ_e in the order of 1 nsec. From the point of view of fitting, it is the long internal correlation time that allows separation of these fast and slow modes of motion. The two-mode motion is clearly not a property of the whole of the molecule as can be seen from the presence of residues with similarly long τ_e but which do not exhibit the fast mode of motion (residue Lys29 in strand D and His50 in the FG loop). In contrast to the varied dynamics of MCP~1, in CR1~16 only five residues require a value for τ_e—in all cases but one (Cys963), the values are small and a fast chemical exchange (motion on 10^{-6} to 10^{-3} sec timescale) component, R_{ex}, is also present.

Strands B, D, E, and F of MCP~1 each contain one residue that is in chemical exchange, whereas each of the three amino acid residues of strand G (residues 51–53), and the preceding residue, also require an R_{ex} component. In the case of Thr51, the signal is line-broadened to the extent that the heteronuclear NOE could not be measured accurately although chemical exchange is clearly present—the fit yielded $R_{ex} = 16\ \mathrm{sec}^{-1}$, but the model was not subject to an F-test. Chemical exchange is also implied by the lack, or weakness, of HSQC peaks for Thr49 and Trp52 (backbone NH). These observations emphasize the atypical nature of backbone dynamics within strand G of MCP~1. The fact

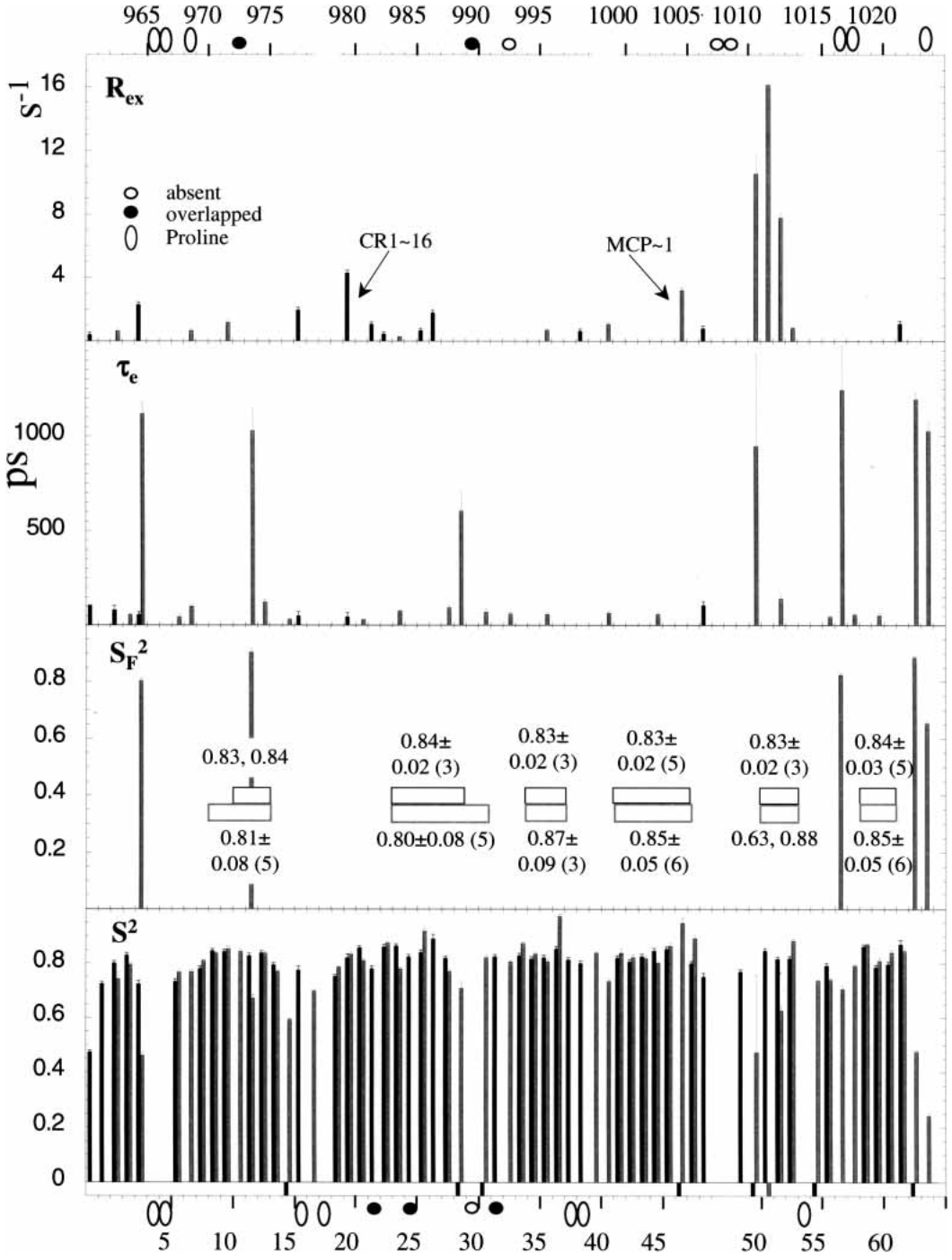

Figure 4. Comparison of model-free data. Model-free data plotted as in Fig. 3 to allow comparison of equivalent residues. Residue numbers on the *bottom* axis refer to MCP; on the *top* axis, to CR1. Oval shape indicates Pro; open and filled circles indicate missing and overlapped HSQC peaks, respectively. Where data could not be fitted, a negative bar is drawn in the lowest plot. White rectangles indicate positions of β-strands in CR1~16 (*upper* set) or MCP~1 (*lower* set), with mean S^2 values ± SD (and number of residues fitted). Black bars used for CR1~16 data; shaded ones, for MCP~1 data. The four panels (from the *top*) show R_{ex}, τ_e, S_F^2, and S^2 values, respectively.

that residue D47, lying at the end of strand F, also requires a R_{ex} parameter suggests a hinge-like movement of the short MCP~1 FG loop pivoting at Asp47 and His50. The turn prior to strand B and the EF loop of MCP~1 might also exhibit this 10^{-6} to 10^{-3} sec timescale hinge-like motion.

Only two of the 10 CR1~16 residues that appear to un-

dergo some degree of 10^{-6} to 10^{-3} sec timescale motion align with those residues in MCP~1 that were also fitted by using R_{ex} parameters. The region between strands B and D contains four of the 10 such residues (Thr978, Ile980, Val982, and Gly983). Thr978, which is in the hypervariable loop, and Ile980, which has a side chain that interacts with module 15 in CR1~15,16, have substantial R_{ex} components. Both have T_2s that are relatively higher in the presence of module 15, indicating some context dependency. Only two (Ile986 and Thr987) of the 10 R_{ex}-requiring residues are found in a strand. In the native sequence, Thr987 is an Asn and is glycosylated; thus, it and its neighbor might be expected to have different relaxation properties. Two amino acids within the CR1~16 FG loop (Gly1008 and Asn1009), like Thr49 of MCP~1, do not exhibit ^{1}H-^{15}N HSQC peaks at all. These are preceded by Ser1007 that has an R_{ex} component. Thus, in both modules, the FG loops, which differ in length, contain amino acid residues that exhibit 10^{-6} to 10^{-3} sec timescale motion.

In summary with regard to R_{ex}, there are some similarities in terms of backbone 10^{-6} to 10^{-3} sec timescale motion between these two examples of CCP modules. Overall, however, there appears to be little equivalence in the types of motion exhibited by the structurally equivalent regions. This is emphasized in Figure 4.

Discussion

Module structures and dynamics are largely independent of context

The current study focuses on individual CCP modules in order to facilitate and enhance the reliability of the extended model-free approach to the fitting of relaxation data. It cannot, however, be assumed a priori that the structures of single CCP modules are identical to their structures (solved previously) within the contexts of module-pairs, and the same caveat applies to backbone dynamics. Indeed, literature precedent suggests grounds for caution in this respect (Kirkitadze and Barlow 2001). Therefore our demonstration that structure, and dynamics in the case of CR1~16, of the isolated modules are by-and-large representative of their structure (and dynamics) in the presence of neighboring modules was critical. It implies that the current study of the backbone dynamics of individual modules sheds light on motion within the CCP modules of the intact, functional, parent protein.

The observation that isolated MCP~1 with a single GlcNAc (at Asn49) has the same structure in solution that it has in the crystal lattice when part of MCP~1,2 and with the larger N-glycan, is noteworthy. The implied lack of a clear structural role for the sugar moiety of MCP~1 is consistent with its reported functional dispensability (Maisner et al. 1996) but intriguing in the light of the conservation of this N-glycosylation motif of MCP in a range of species (Liszewski et al. 1998). Interestingly, MCP~2 does, in contrast, appear to require its functionally important N-glycan for structural integrity (Liszewski et al. 1998; Herbert et al. 2002).

Structurally equivalent residues in two examples of CCP modules undergo different motions

Given the variations in primary, secondary, and tertiary structure between the two CCP modules in this study, differences in backbone dynamics would be expected, particularly when the sequences and structures diverge most. But, on the contrary, the hypervariable loops of the two CCPs in this study, although different in length, displayed very similar dynamic features, as did the variable-length FG loops. On the other hand, significant differences in mobility are observed in regions, such as the BDF triple-stranded sheet, that are well-conserved between these two modules and across CCP modules generally (Figs. 4, 5). The various kinds of mobility displayed by the two modules might therefore be linked to the respective roles each plays in the biological functions of the parent proteins.

Implication for biological function

A contributing factor to the differences in dynamics observed in this study might be the selection of a terminal CCP module (MCP~1) for comparison with a CCP module

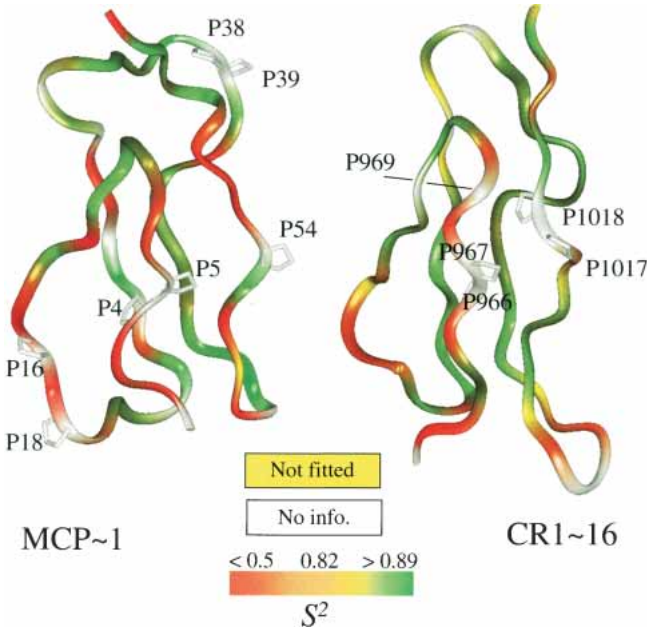

Figure 5. Model free analysis in the context of the 3D structures. Ribbon representations of the two CCP modules color-coded according to the S^2 value of individual residues. Same view as in Fig. 1B. Prolines (with side chains drawn as sticks) and other residues for which no relaxation data are available are colored white; residues that could not be fitted are in yellow. Lowest values of S^2 (most mobile) are in red, and the highest values are in green (colors are merged; see color bar). For orientation, prolines are numbered according to sequence position.

(CR1~16) that in its native context lies close to the middle of a train of 30 modules. Although MCP~1 might have evolved purely as a versatile molecular recognition module, the evolution of CR1~16 would have been constrained by architectural considerations, namely, the need to contribute toward a specific level of overall flexibility in CR1. This could explain why CR1~16 has a more rigid framework than does MCP~1.

A further, not unconnected, consideration is that these two modules use different parts of their surfaces as interaction sites and have different binding partners. A correlation between backbone dynamics and the ability to interact specifically with other proteins has been observed many times. For example, residues involved in receptor binding of the chemokine eotaxin, in the substrate binding loop of nematode anticoagulant binding protein c2, and in protein–protein contacts in assembly of a bacterial chemotaxis signaling complex, exhibit motions on several timescales (Crump et al. 1999; Duggan et al. 1999; Griswold and Dahlquist 2002), and protein interaction sites of the *Escherichia coli* chaperone protein DnaJ, and the DNA-binding domains of the estrogen receptor, and the transcription factor PU.1 exhibit 10^{-6} to 10^{-3} sec timescale motions (Huang et al. 1999; Wikstrom et al. 1999; McKercher et al. 2003).

As may be judged from Figure 4, strands B, D, and F, that make up one face of CR1~16 are characterized by residues with large-order parameters, symptomatic of little mobility. The only two residues on this "BDF" face requiring a substantial R_{ex} parameter are the mutated residue Thr987 (normally Asn987) at the N-glycosylation site and its neighbor Ile986. On the basis of existing mutagenesis information, this face appears not to be involved in interactions with C3b, consistent with the presence of the functionally nonessential N-glycosylation site at Asn987 (Krych et al. 1998; Kirkitadze et al. 1999c; Smith et al. 2002).

Residues Lys964, Asn1009, and Lys1016 of CR1~16, which are critical to binding, lie on the opposite face of CR1~16 to the BDF face. This consists of the FG loop, strand G, and the extended region running from the first Cys (963) to the turn (Val970–Gly972) before strand B. Residues on this face have a range of dynamic properties. Strand G of CR1~16 is well defined by homonuclear NOEs and exhibits little backbone motion, whereas residues in the FG loop lack HSQC peaks (probably due to exchange-broadening) or exhibit low S^2 values, consistent with mobility on several timescales. The N-terminal 963–970 region encompasses three Pro (for which no dynamical information is available) and contains several residues that have low S^2 values, including one (Thr965) that requires a R_{ex} component. This specific protein-binding surface therefore has the ability to undergo structural perturbations of a range of amplitudes and on several timescales. In this respect, its dynamics resemble those of a growing list of protein–protein interaction sites (see above).

Residues on all three modules of CR1 site 2 have been implicated in binding C3b (Krych et al. 1994, 1998). In addition to the dynamics within module 16 reported here, flexibility exists between modules 16 and 17 and, to a lesser extent, between modules 15 and 16 (Smith et al. 2002). Furthermore, all amide protons of CCP-modules looked at, to date, exchange with D_2O within minutes or hours, suggesting conformational mobility on this timescale as well. An electrostatic contribution to the interaction is suggested by mutagenesis (Liszewski et al. 2000). Therefore, recognition and binding of C3b, the primary function of site 2, could proceed via a relatively nonspecific electrostatic attraction followed or accompanied by a conformational adjustment or rigidification in CR1 to achieve complementarity with a binding surface on the C3b molecule that could also allow H-bond formation and/or hydrophobic interactions. Such an "induced fit" mechanism involving site 2 might impose an entropic cost on the affinity of the interaction, which is reported to be in the range of 1 μM (Frade and Strominger 1980; Weisman et al. 1990), but could enhance on-rate and/or specificity. Analysis of the backbone dynamics of existing mutants, and further rational mutagenesis aimed at altering dynamic properties, will help to test this hypothesis.

The so-called hypervariable loop (residues 976–982) that projects laterally from the CR1~16 module is another dynamic feature, as is the equivalent region of MCP~1 (residues 14–22). Hypervariable loops of CCPs in general have been tentatively suggested as potential direct interaction sites on the basis of their high sequence variability and exposed nature (away from the interfaces with other modules). The current study adds weight to that hypothesis by demonstrating that these two examples contains a high concentration of residues that are dynamic either on the 10^{-12} to 10^{-9} or 10^{-6} to 10^{-3} sec timescales. Although the hypervarible region of CR1~16 appears not to be important for C3b-binding or cofactor activity, it could well be involved in some other binding activity. For example, site 2 of CR1 has been shown to interact with the malarial adhesin PfEMP1 (for review, see Krych-Goldberg et al. 2002), a key factor in pathogenicity because it enables clumping, or rosetting, of infected and noninfected erythrocytes. Functional assay of mutations in the hypervariable loop would allow exploration of its possible involvement in this interaction, which is a potential target for therapy.

The color-coding of Figure 5 emphasizes that MCP~1 has, overall, more residues with low S^2 values than does CR1~16. Unlike CR1~16, it does not have one relatively rigid face and another mobile one. The most mobile regions of CR1~16 are also mobile in MCP~1, but there are additional mobile features in MCP~1. In particular, strand G and the slightly longer region between strands G and H are conspicuously more dynamic, on both fast and slow timescales (Fig. 4) than are the equivalent regions of CR1~16.

As pointed out above, the two modules also show quite striking differences in the dynamic properties of strand D. The face of the module involving strands D, E, and F, together with the FG loop, and the hypervariable loop (after strand B) are thought to form the interaction surface for the measles virus hemagglutinin protein (Manchester et al. 1997). An overlapping site including the FG loop, strand G, and the G to H region was identified as the region of MCP~1 contributing to binding of C4b (Liszewski et al. 2000). All of these are mobile on a range of timescales. As with the C3b-interaction of CR1, this information is consistent with an induced-fit mechanism of MCP binding to both complement and viral ligands. It is possible that the ability of MCP to bind the two very diverse ligands is a result in part of its flexibility.

In conclusion, it has been shown that NMR relaxation studies of isolated modules provide insight into local mobility within RCA proteins. Previously established binding patches appear to correlate with dynamic surface regions of two CCP modules. The current work suggests mutagenesis studies to further define the binding mechanisms and to explore the potential of further mobile residues to form as-yet-unrecognized binding sites in CR1~16. Such an approach could be extended to identifying binding sites in other examples of CCP modules in RCA proteins and in the wider family of functionally diverse CCP module–containing proteins.

Materials and methods

Production of MCP~1

A 71-residue fragment containing amino acids (aa) 1–64 of the native human MCP sequence (MCP~1) plus, at the N terminus, three additional residues (Y V E), due to a cloning artefact, and four residues (F S D A), from the signal sequence, was expressed in *Pichia pastoris*. A DNA fragment encoding MCP~1 was amplified from MCP cDNA (BC2 isoform) by PCR. Directional cloning of the fragment in-frame with the α-factor secretion sequence in the pPIC9 vector was carried out, and the linearized plasmid was transformed into *P. pastoris* KM71. Transformants were selected on histidine-deficient media.

Based on small-scale MCP~1 expression screens, the highest-expressing clone was selected for scale-up and ^{15}N-enrichment. The cell-free supernatant from shaker-flask growths, with ^{15}N-ammonium sulphate as sole nitrogen source, was concentrated and loaded onto an anion-exchange column. Part-purified MCP~1 was subsequently incubated with endoglycosidase H_f (5 mU.mg^{-1} protein) for 16 h at 37°C, then isolated by reverse-phase chromatography. A concavalin A–Sepharose column was used to remove residual carbohydrate. Finally, the protein was desalted and concentrated by RP-HPLC. Protein identity and homogeneity was verified by N-terminal sequencing and electrospray mass spectrometry. The mass determined (8541.8 ± 0.2 D) corresponded closely to that calculated (8541.6) assuming disulphide formation, and allowing for a single N-acetylglucosamine moiety attached to Asn49 resulting from endoglycosidase treatment of the hyperglycosylated *P. pastoris* product. Typically, 6 to 8 mg of purified protein were obtained per liter of culture.

Production of CR1~16

The CR1~16 construct contained 68 residues, including E A E A, from the *P. pastoris* signal peptide at the N terminus and native residues corresponding to 961–1024 of CR1, except that Asn987—an N-glycosylation site—was mutated to Thr (molecular weight = 7312 D). Production and purification of ^{15}N-CR1~16 was as described previously (Kirkitadze et al. 1999c).

NMR experiments

Samples for NMR consisted of 1.0 mM ^{15}N-MCP~1 and 50 mM potassium phosphate (pH 6.0), or 0.5 mM ^{15}N-CR1~16 and 25 mM potassium phosphate (pH 6.0). NMR spectra were recorded at 37°C on a Varian INOVA-600 spectrometer equipped with a 5-mm z-gradient triple-resonance probe.

Assignment was obtained from two-dimensional (2D) total correlation spectroscopy (TOCSY) and 3D ^{15}N-edited TOCSY experiments with 35 (or 38)-msec and 70 (or 69.5)-msec mixing times, respectively, for MCP~1 (or CR1~16). Band-selective 2D TOCSY-TOCSY and 2D TOCSY–NOE spectroscopy (NOESY) experiments (D. Uhrin, unpubl.) assisted identification of Pro spin systems in MCP~1 due to spectral simplification and better resolution.

NOE connectivities were established from ^{15}N-edited 3D NOESY-HSQC and 2D NOESYs with 100 (or 150)-msec and 150 (or 100)-msec mixing times, respectively, for MCP~1 (or CR1~16). The $J_{HNH\alpha}$ coupling constants in MCP~1 were determined from a HNHA experiment (Kuboniwa et al. 1994). Amide proton exchange in MCP~1 was monitored in HSQC spectra of initially protonated samples dissolved in D_2O to establish H-bond donors—after 28 minutes, 12 resonances were observed—these had largely disappeared after 1 h (data not shown).

The ^{15}N T_1 and T_2 relaxation times were measured according to the method of Kay et al. (1992) and as described previously (Smith et al. 2002). The relaxation delays used were as follows: MCP~1 T_1s, 6.75 (twice), 546, 601, and 655 msec; MCP~1 T_2s, 16.3, 32.6, 163, 179, and 195 msec; CR1~16 T_1s, 12.2, 132, 274, 601, and 1091 msec; and CR1~16 T_2s, 16, 32, 64, 128, 196, and 286 msec. Heteronuclear (^{1}H-^{15}N) NOEs were measured as described previously (Smith et al. 2002).

NOE assignments and structure calculations

Spectral quality for both modules in terms of line widths and overlap was similar, but fewer ^{1}H-^{1}H NOEs were identified in the weaker CR1~16 sample due to signal-to-noise considerations, and amide proton-exchange estimates were not done for CR1~16. Spectra were peak-picked and integrated within ANSIG (Kraulis 1989). A total of 1441 (or 885) ^{1}H-^{1}H NOE peaks were assigned for MCP~1 (or CR1~16). These NOEs, along with distance restraints representing eight inferred H-bonds for MCP~1, and two disulphides (in both modules) were used as input for simulated annealing within the 'Crystallography and NMR systems' program (Brunger et al. 1998). Cross peaks were classified as follows: strong (≡ interproton distances of <2.7 Å), medium (<3.3 Å), weak (<4.5 Å in MCP~1; <5.0 Å in CR1~16), or very weak (<6.0 Å). Stereochemical assignments were dealt with as described (Bramham et al. 2002). For each module, a total of 60 structures was

calculated, of which 20 were selected on the basis of lowest energy. Structure-determination statistics are presented in Table 1.

Relaxation data analysis

The symmetry of the overall rotational diffusion was established by correlating T_1/T_2 ratios to both NMR-derived, and (if available) X-ray–derived, structures. Only those residues not undergoing local motion (i.e., with heteronuclear NOE >0.65, and no indication of chemical exchange according to Barbato et al. criteria [1992]) were used for fitting. When using nearest-to-mean MCP~1 and CR1~16 NMR structures, diffusion could be represented in both cases by isotropic correlation times (Table 2); there was no significant improvement when axially symmetric diffusion was introduced. Use of the alternative structure of MCP~1 derived from the MCP~1,2 crystal structure, however, resulted in a significant improvement of the fit with axially symmetric diffusion, yielding $D_{||}/D_{\perp} = 1.35$ (Table 2). The diffusion of MCP~1 was modeled from the atomic coordinates within the program HYDROPRO (de la Torre et al. 2000). The axial ratio $D_{||}/D_{\perp} =$ was modelled to be 1.6 with deviation from ideal axial symmetry <2%. The lower $D_{||}/D_{\perp} =$ calculated on the basis of NMR relaxation is likely the result of hydration, which is not fully included in the HYDROPRO suite.

The relaxation data for the two modules were then analyzed according to the extended model-free approach (Lipari and Szabo 1982). Appropriate models were chosen by using an iterative fitting procedure (Fig. 4; Mandel et al. 1995). This started with the simplest model (in which a single motional parameter is adequate to fit the experimentally measured relaxation rates) and invoked increasingly complex models until the proposed model agreed with the experimental data within 90% confidence limits. The statistical significance of each additional parameter was assessed by using an F-statistic with $\alpha = 0.20$ critical value.

Acknowledgments

This project was supported by the Darwin Trust (studentship to K.B.), the UK Medical Research Council (fellowship to K.B.), the Wellcome Trust-funded Edinburgh Protein Interaction Centre, and the NIH grant R01 A141592 to J.P.A.

The publication costs of this article were defrayed in part by payment of page charges. This article must therefore be hereby marked "advertisement" in accordance with 18 USC section 1734 solely to indicate this fact.

Note added in proof

Atomic coordinates for MCP~1 and CR1~16 have been deposited with the PDB, accession numbers 1NWV and 1PPQ, respectively.

References

Barbato, G., Ikura, M., Kay, L.E., Pastor, R.W., and Bax, A. 1992. Backbone dynamics of calmodulin studied by ^{15}N relaxation using inverse detected two-dimensional NMR spectroscopy: The central helix is flexible. *Biochemistry* **31:** 5269–5278.

Barlow, P.N., Steinkasserer, A., Norman, D.G., Kieffer, B., Wiles, A.P., Sim, R.B., and Campbell, I.D. 1993. Solution structure of a pair of complement modules by nuclear magnetic resonance. *J. Mol. Biol.* **232:** 268–284.

Birmingham, D.J. and Hebert, L.A. 2001. CR1 and CR1-like: The primate immune adherence receptors. *Immunol. Rev.* **180:** 100–111.

Bork, P., Downing, A.K., Kieffer, B., and Campbell, I.D. 1996. Structure and distribution of modules in extracellular proteins. *Q. Rev. Biophys.* **29:** 119–167.

Bramham, J., Hodgkinson, J.L., Smith, B.O., Uhrin, D., Barlow, P.N., and Winder, S. 2002. Solution structure of the calponin CH domain and fitting to the helical reconstruction of F-actin:calponin. *Structure* **10:** 249–258.

Brunger, A.T., Adams, P.D., Clore, G.M., DeLano, W.L., Gros, P., Grosse-Kunstleve, R.W., Jiang, J.-S., Kuszewski, J., Nilges, N., Pannu, N.S., et al. 1998. Crystallography and NMR system (CNS): A new software system for macromolecular structure determination. *Acta Crystallogr. D* **54:** 905–921.

Casasnovas, J.M., Larvie, M., and Stehle, T. 1999. Crystal structure of two CD46 domains reveals an extended measles virus-binding surface. *EMBO J.* **18:** 2911–2922.

Crump, M.P., Spyracopoulos, L., Lavigne, P., Kim, K.S., Clark-Lewis, I., and Sykes, B.D. 1999. Backbone dynamics of the human CC chemokine eotaxin: Fast motions, slow motions, and implications for receptor binding. *Protein Sci.* **8:** 2041–2054.

de la Torre, J.G., Huertas, J., and Carrasco, B. 2000. Calculation of hydrodynamic properties of proteins from their atomic structure. *Biophys. J.* **78:** 719–730.

Duggan, B.M., Dyson, H.J., and Wright, P.E. 1999. Inherent flexibility in a potent inhibitor of blood coagulation, recombinant nematode anticoagulant protein c2. *Eur. J. Biochem.* **2:** 539–548.

Frade, R. and Strominger, J. 1980. Binding of soluble ^{125}I-human C3b, the third component of complement, to specific receptors in human cultured B lymphoblastoids cells: Characterization of a low affinity interaction. *J. Immunol.* **125:** 1332–1339.

Griswold, I.J. and Dahlquist, F.W. 2002. The dynamic behavior of CheW from *Thermotoga maritima* in solution, as determined by nuclear magnetic resonance: Implications for potential protein–protein interaction sites. *Biophys. Chem.* **101–102:** 359–373.

Henderson, C., Bromek, K., Smith, B.O., Uhrin, D., and Barlow, P.N. 2001. Structure and dynamics of the central modules of a poxvirus complement control protein. *J. Mol. Biol.* **307:** 323–339.

Herbert, A., O'Leary, J., Krych-Goldberg, M., Atkinson, J.P., and Barlow, P.N. 2002. Three-dimensional structure and flexibility of proteins of the RCA family: A progress report. *Biochem. Soc. Trans.* **30:** 990–996.

Hsu, E.C., Sabatinos, S., Hoedemaeker, F.J., Rose, D.R., and Richardson, C.D. 1999. Use of site-specific mutagenesis and monoclonal antibodies to map regions of CD46 that interact with measles virus H protein. *Virology* **258:** 314–326.

Huang, K., Ghose, R., Flanagan, J.M., and Prestegard, J.H. 1999. Backbone dynamics of the N-terminal domain in *E. coli* DnaJ determined by ^{15}N- and ^{13}CO-relaxation measurements. *Biochemistry* **38:** 10567–10577.

Ishima, R. and Torchia, D.A. 2000. Protein dynamics from NMR. *Nat. Struct. Biol.* **7:** 740–743.

Kay, L.E., Torchia, D.A., and Bax, A. 1989. Backbone dynamics of proteins as studied by ^{15}N inverse detected heteronuclear NMR spectroscopy: Application to staphylococcal nuclease. *Biochemistry* **28:** 8972–8979.

Kay, L.E., Nicholson, L.K., Delaglio, F., Bax, A., and Torchia, D.A. 1992. Pulse sequences for removal of effects of cross correlation between dipolar and chemical shift anisotropy relaxation mechanisms on the measurement of heteronuclear T_1 and T_2 values in proteins. *J. Magn. Reson.* **97:** 359–375.

Kirkitadze, M.D. and Barlow, P.N. 2001. Structure and flexibility of the multidomain proteins that serve as regulators of complement activation. *Immunol. Rev.* **180:** 146–161.

Kirkitadze, M.D., Dryden, D.T.F., Kelly, S.M., Price, N.C., Wang, X., Krych, M., Atkinson, J.P., and Barlow, P.N. 1999a. Co-operativity between modules within a C3b-binding site of complement receptor type 1. *FEBS Lett.* **459:** 133–138.

Kirkitadze, M.D., Henderson, C., Price, N.C., Kelly, S.M., Mullin, N.P., Parkinson, J., Dryden, D.T.F., and Barlow, P.N. 1999b. Central modules of the Vaccinia virus complement control protein are not in extensive contact. *Biochem. J.* **343:** 167–175.

Kirkitadze, M.D., Krych, M., Uhrin, D., Dryden, D.T.F., Cooper, A., Wang, X., Hauhart, R., Atkinson, J.P., and Barlow, P.N. 1999c. Independently melting modules and highly structured intermodular junctions within complement receptor type 1. *Biochemistry* **38:** 7019–7031.

Kraulis, P.J. 1989. ANSIG: A program for the assignment of protein ^1H 2D NMR spectra by interactive graphics. *J. Magn. Reson.* **24:** 627–633.

———. 1991. MOLSCRIPT: A program to produce both detailed and schematic plots of protein structures. *J. Appl. Crystallogr.* **24:** 946–950.

Krych, M., Hourcade, D., and Atkinson, J.P. 1991. Sites within the complement C3b/C4b receptor important for the specificity of ligand binding. *Proc. Natl. Acad. Sci.* **88:** 4353–4357.

Krych, M., Clemenza, L., Howdeshell, D., Hauhart, R., Hourcade, D., and Atkinson, J.P. 1994. Analysis of the functional domains of complement

receptor-type-1 (C3b/C4b receptor, CD35) by substitution mutagenesis. *J. Biol. Chem.* **269:** 13273–13278.

Krych, M., Hauhart, R., and Atkinson, J.P. 1998. Structure-function analysis of the active sites of complement receptor type 1. *J. Biol. Chem.* **273:** 8623–8629.

Krych-Goldberg, M. and Atkinson, J.P. 2001. Structure-function relationships of complement receptor type 1. *Immunol. Rev.* **180:** 112–122.

Krych-Goldberg, M., Moulds, J.M., and Atkinson, J.P. 2002. Human complement receptor type 1 (CR1) binds to a major malarial adhesin. *Trends Mol. Med.* **8:** 531–537.

Kuboniwa, H., Grzesiek, S., Delaglio, F., and Bax, A. 1994. Measurement of HNHA J-couplings in calcium-free calmodulin using new 2D and 3D water-flip-back methods. *J. Biomol. NMR* **4:** 871–878.

Lipari, G. and Szabo, A. 1982. Model-free approach to the interpretation of nuclear magnetic resonance relaxation in macromolecules, 1: Theory and range of validity. *J. Am. Chem. Soc.* **104:** 4546–4559.

Liszewski, M.K., Post, T.W., and Atkinson, J.P. 1991. Membrane cofactor protein (MCP or CD46): Newest member of the regulators of complement activation gene cluster. *Annu. Rev. Immunol.* **9:** 431–455.

Liszewski, M.K., Leung, M.K., and Atkinson, J.P. 1998. Membrane cofactor protein: Importance of N- and O-glycosylation for complement regulatory function. *J. Immunol.* **161:** 3711–3718.

Liszewski, M.K., Leung, M., Cui, W., Subramanian, V.B., Parkinson, J., Barlow, P.N., Manchester, M., and Atkinson, J.P. 2000. Dissecting sites important for complement regulatory activity in membrane cofactor protein (MCP; CD46). *J. Biol. Chem.* **275:** 37692–37701.

Maisner, A., Alvarez, J., Liszewski, M.K., Atkinson, D.J., Atkinson, J.P., and Herrler, G. 1996. The N-glycan of the SCR 2 region is essential for membrane cofactor protein (CD46) to function as a measles virus receptor. *J. Virol.* **70:** 4973–4977.

Manchester, M., Gairin, J.E., Patterson, J.B., Alvarez, J., Liszewski, M.K., Eto, D.S., Atkinson, J.P., and Oldstone, M.B. 1997. Measles virus recognizes its receptor, CD46, via two distinct binding domains within SCR1–2. *Virology* **233:** 174–184.

Mandel, A.M., Akke, M., and Palmer, A.G. 1995. Backbone dynamics of *Escherichia coli* ribonuclease HI: Correlations with structure and function in an active enzyme. *J. Mol. Biol.* **246:** 144–163.

McKercher, S.R., Lombardo, C.R., Bobkov, A., Jia, X., and Assa-Munt, N. 2003. Identification of a PU.1-IRF4 protein interaction surface predicted by chemical exchange line broadening. *Proc. Natl. Acad. Sci.* **100:** 511–516.

Medof, M.E., Lublin, D.M., Holers, V.M., Ayers, D.J., Getty, R.R., Leykam, J.F., Atkinson, J.P., and Tykocinski, M.L. 1987. Cloning and characterization of cDNAs encoding the complete sequence of decay-accelerating factor of human complement. *Proc. Natl. Acad. Sci.* **84:** 2007–2011.

Murthy, K., Smith, S.A., Ganesh, V.K., Judge, K.W., Mullin, N., Barlow, P.N., Ogata, C.M., and Kotwal, G. 2001. Crystal structure of a complement control protein that regulates both pathways of complement activation and binds heparan sulfate proteoglycans. *Cell* **104:** 301–311.

Pangburn, M.K. 2000. Host recognition and target differentiation by factor H, a regulator of the alternative pathway of complement. *Immunopharmacology* **49:** 149–157.

Reid, K.B.M. and Day, A.J. 1988. Structure–function relationships of the complement components. *Immunol. Today* **10:** 177–180.

Smith, B.O., Mallin, R.L., Krych-Goldberg, M., Wang, X., Hauhart, R.E., Bromek, K., Uhrin, D., Atkinson, J.P., and Barlow, P.N. 2002. Structure of the C3b-binding site of CR1 (CD35), the immune adherence receptor. *Cell* **108:** 769–780.

Uhrinova, S., Lin, F., Ball, G., Bromek, K., Uhrin, D., Medof, M.E., and Barlow, P.N. 2003. Solution structure of a functionally active fragment of decay-accelerating factor. *Proc. Natl. Acad. Sci.* **100:** 4718–4723.

Walport, M.J. 2001. Complement: Second of two parts. *N. Engl. J. Med.* **344:** 1140–1144.

Wand, A.J. 2001. Dynamic activation of protein function: A view emerging from NMR spectroscopy. *Nat. Struct. Biol.* **8:** 926–931.

Weisman, H.F., Bartow, T., Leppo, M.K., Marsh Jr., H., Carson, G.R., Concino, M.F., Boyle, M.P., Roux, K.H., Weisfeldt, M.L., and Fearon, D.T. 1990. Soluble human complement receptor type 1: In vivo inhibitor of complement suppressing post-ischemic myocardial inflammation and necrosis. *Science* **249:** 146–151.

Wikstrom, A., Berglund, H., Hambraeus, C., van den Berg, S., and Hard, T. 1999. Conformational dynamics and molecular recognition: Backbone dynamics of the estrogen receptor DNA-binding domain. *J. Mol. Biol.* **289:** 963–979.

Williams, P., Chaudhry, Y., Goodfellow, I.G., Billington, J., Powell, R., Spiller, O.B., Evans, D.J., and Lea, S. 2003. Mapping CD55 function: The structure of two pathogen-binding domains at 1.7 Ångstrom. *J. Biol. Chem.* **278:** 10691–10696.